Title

Electronic Structure of Two Catalytic States of the [FeFe] Hydrogenase H-Cluster As Probed by Pulse Electron Paramagnetic Resonance Spectroscopy

Journal

Inorganic Chemistry, 57(17)

ISSN

0020-1669

Authors

Rao, Guodong
Britt, R David

Publication Date

2018-09-04

DOI

10.1021/acs.inorgchem.8b01557

Peer reviewed

HHS Public Access

Author manuscript

Inorg Chem. Author manuscript; available in PMC 2019 February 07.

Published in final edited form as:

Inorg Chem. 2018 September 04; 57(17): 10935–10944. doi:10.1021/acs.inorgchem.8b01557.

Electronic structure of two catalytic states of the [FeFe] hydrogenase H-cluster as probed by pulse electron paramagnetic resonance spectroscopy

Guodong Rao and **R. David Britt**

Department of Chemistry, University of California, Davis, CA 95616

Abstract

The active site of the [FeFe] hydrogenase (HydA1), the H-cluster, is a 6-Fe cofactor that contains CO and CN^- ligands. It undergoes several different oxidation and protonation state changes in its catalytic cycle to metabolize H_2. Among them, the well-known H_{ox} state and the recently identified H_{hyd} state are thought to be directly involved in H_2 activation and evolution, and they are both EPR active with net spin $S = 1/2$. Herein, we report the pulse electronic paramagnetic spectroscopic investigation of these two catalytic states in *Chlamydomonas reinhardtii* HydA1 (*Cr*HydA1). Using an *in vitro* biosynthetic maturation approach, we site-specifically installed ^{13}C into the CO or CN^- ligands and ^{57}Fe into the $[2Fe]_H$ subcluster of the H-cluster in order to measure the hyperfine couplings to these magnetic nuclei. For H_{ox}, we measured ^{13}C hyperfine couplings (^{13}CO a_{iso} of 25.5, 5.8, and 4.5 MHz) corresponding to all three CO ligands in the H-cluster. We also observed two ^{57}Fe hyperfine couplings (^{57}Fe a_{iso} of ~17 MHz and 5.7 MHz) arising from the two Fe atoms in the $[2Fe]_H$ subcluster. For H_{hyd}, we only observed two distinct ^{13}CO hyperfine interaction (^{13}CO a_{iso} of 0.16 and 0.08 MHz), and only one for $^{13}CN^-$ (^{13}CN a_{iso} of 0.16 MHz)—the couplings to the $^{13}CO/^{13}CN^-$ on the distal Fe of $[2Fe]_H$ may be too small to detect. We also observed a very small (< 0.3 MHz) ^{57}Fe HFI from the labeled $[2Fe]_H$ subcluster, and four ^{57}Fe HFI from the labeled $[4Fe\text{-}4S]_H$ subcluster (^{57}Fe a_{iso} of 7.2, 16.6, 28.2, and 35.3 MHz). These hyperfine coupling constants are consistent with the previously proposed electronic structure of the H-cluster at both H_{ox} and H_{hyd} states, and provide a basis for more detailed analysis.

Graphical Abstract

Correspondence to: R. David Britt.

Supporting Information

Supporting information available: X- and Q-band HYSCORE spectra of $[^{13}CO]\text{-}H_{ox}$; Q-band Davies ENDOR spectrum of $[^{13}CO]\text{-}H_{ox}$-CO; VMT Mims-ENDOR spectra of $[^{13}CO]\text{-}H_{hyd}$; simulation of Q-band ENDOR and HYSCORE spectra of Fe_B feature; simulation of Q-band ^{57}Fe ENDOR spectra of $[2^{57}Fe]\text{-}H_{ox}$; Q-band HYSCORE spectrum of $[2^{57}Fe]\text{-}H_{hyd}$ at $g = 2.008$ and simulation; comparison of X-band CW EPR spectra of H_{hyd}, $[2^{57}Fe]$-, and $[6^{57}Fe]\text{-}H_{hyd}$; Simulation of field-dependent Q-band HYSCORE spectra of $[6^{57}Fe]\text{-}H_{hyd}$

Notes

The authors declare no conflict of interest.

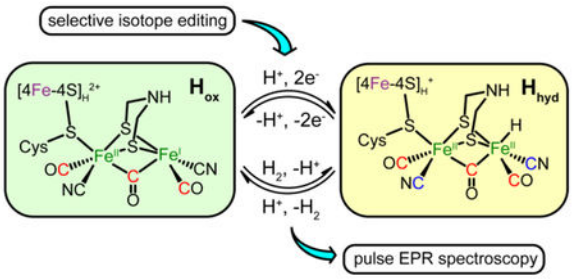

Introduction

Hydrogenases are used by nature to catalyze the reversible conversion between H_2 and H^+/e^-.[1–2] In [FeFe] hydrogenases, the catalytic center "H-cluster" consists of a tetracysteine (Cys) coordinated $[4Fe\text{-}4S]_H$ subcluster linked through one Cys residue thiol to an organometallic $[2Fe]_H$ subcluster that has CO and CN^- ligands along with an azadithiolate (adt) ligand that bridges the two iron ions (Scheme 1).[3–6] The H-cluster has been shown to adopt different oxidation and protonation states that have unique spectroscopic properties: the most oxidized state, H_{ox}, the one-electron reduced state (H_{red}, $H_{red}H^+$, H_{red}*), and the two-electron reduced state (H_{sred}, $H_{sred}H^+$, H_{sred}*).[7–12] Most recently, another state of the H-cluster with a terminal iron hydride, H_{hyd}, has been identified in *Chlamydomonas reinhardtii* HydA1 (*Cr*HydA1), in the wild-type enzyme and several variants.[13–17] Importantly, H_{hyd} is considered to be one of the key state in the catalytic cycle of [FeFe] hydrogenase,[13, 15, 18] as the terminal hydride is thought to coordinate with the pendant amine of the adt ligand to form a frustrated Lewis pair that is necessary for H_2 activation and evolution.[19–20] The full characterization of H_{hyd} is therefore crucial to further understand the mechanism of H-cluster-based catalysis.

Both $S = 1/2$ EPR-active states, H_{ox} and H_{hyd}, represent different forms of the H-cluster in the proposed catalytic cycle of [FeFe] hydrogenase (Scheme 1).[15–16] Results from Mössbauer spectroscopy, electron nuclear double resonance (ENDOR) spectroscopy, and DFT calculations support a $[4Fe\text{-}4S]_H^{2+}$ -$[Fe^{II}Fe^{I}]_H$ configuration for H_{ox}, with a net spin of $S = 1/2$ that is primarily localized on the mixed-valance $[2Fe]_H$, and less spin density on the $[4Fe\text{-}4S]_H^{2+}$ (which would be a diamagnetic cluster if isolated from the paramagnetic $[Fe^{II}Fe^{I}]_H$).[12, 21–22] Hyperfine interactions (HFI) for specifically $^{13}CN^-$ and ^{57}Fe -labeled $[2Fe]_H$ have been reported for H_{ox} and its CO-inhibited state, H_{ox}-CO.[23–27] These ^{57}Fe and ^{13}C hyperfine coupling constants have been used to estimate the spin density distribution in the H-cluster. More recently, the ^1H NMR spectrum was also reported for H_{ox}, providing further insights into its electronic structure.[28] Despite these efforts to characterize H_{ox}, questions still remain. One in particular is why only one ^{57}Fe HFI has been detected for the $[2Fe]_H$ of *Clostridium pasteurianum* CpI and *Chlamydomonas reinhardtii* HydA1,[27, 29] yet two distinct HFI for the coordinating $^{13}CN^-$ have been found, one assigned as a ligand to the proximal, nominally Fe^{II} ion (Fe_p) (^{13}C a_{iso} = 4.9 MHz), and one assigned as a ligand to the spin-bearing distal Fe^I (Fe_d) (^{13}C a_{iso} = 27 MHz).[25] Simulations of Mössbauer results also implied that only one large ^{57}Fe HFI should be present in H_{ox}.[12] Similarly in *Desulfovibrio desulfuricans* DdH, while identical ^{57}Fe hyperfine couplings were experimentally measured

for the two Fe sites in $[2Fe]_H$,[30] DFT calculations using a variety of models suggested that their couplings should be significantly different.[31] Clarifying this inconsistency is not only of fundamental interest, but would also shed light in designing molecular models for hydrogenase.

As for H_{hyd}, while the proposed formula of H_{hyd} may be viewed as binding of a terminal hydride on the Fe_d of H_{ox}, previous studies suggested that H_{hyd} adopts a $[4Fe\text{-}4S]_H^+$-$[Fe^{II}Fe^{II}]_H$-H^- configuration, with a net spin of $S = 1/2$ that is now primarily localized on the $[4Fe\text{-}4S]_H$.[16] This assignment is supported by the g-tensor of H_{hyd} ($g = [2.08, 1.94, 1.88]$) that is similar to that found for typical $[4Fe\text{-}4S]^+$ clusters, the presence of two low-spin diamagnetic Fe^{2+} in the $[2Fe]_H$ with small isomer shifts ($\delta = 0.03$ and 0.23 mm/s) as revealed by Mössbauer spectroscopy, as well as by DFT calculations.[15–16] Interestingly, the proposed electronic structure of H_{hyd} is analogous to that of a reaction intermediate we recently trapped in HydG,[32] the enzyme responsible for the early steps of H-cluster bioassembly.[29, 33] Specifically, we identified a $[4Fe\text{-}4S]^+$-$[(Cys)Fe^{II}(CO)(CN)]$ species and observed small ^{13}C (a_{iso} = 0.22 and 0.24 MHz) and ^{57}Fe (a_{iso} = 0.42 MHz) HFI from the specifically labeled ^{13}CO, $^{13}CN^-$ ligands and the low-spin dangler $^{57}Fe^{II}$ respectively.[32] Therefore, we reason that similarly small HFI could be observed for H_{hyd} and these HFI could be used to clearly define the electronic configuration of H_{hyd}.

The Swartz lab has developed an *in vitro* approach to assemble the H-cluster by using apo-hydrogenase (that harbors only the $[4Fe\text{-}4S]_H$), cell lysate of maturation enzymes—HydE, HydF and HydG—responsible for the biosynthesis of the $[2Fe]_H$,[34–36] and necessary substrates/cofactors.[37–39] This “cell free synthesis” method enables us to facilely and precisely install various isotopes into the $[2Fe]_H$[25, 29] In this work, we have taken advantage of this strategy and selectively labeled *Cr*HydA1 with ^{13}CO, $^{13}CN^-$, and ^{57}Fe, allowing us to determine the electronic structures of the H-cluster at both H_{ox} and H_{hyd} states via the HFI of these various magnetic nuclei. These results provide further insights into the structure and function of this unique cofactor.

Methods

General Consideration.

^{57}Fe and, ^{13}C- and ^{15}N- labeled Tyr were purchased from Cambridge Isotope Inc. All other chemicals were from Sigma-Aldrich unless specified. All handling of Fe-S cluster proteins, which includes purification of *Cr*HydA1, preparation of HydE, HydF and HydG lysate, maturation of *Cr*HydA1, and preparation of EPR samples, were carried out in an anaerobic chamber with O_2 level < 1 ppm.

In vitro maturation of *Cr*HydA1.

Maturation experiments were performed according to previous procedure with slight modifications.[29, 37] These experiments required apo-*Cr*HydA1, lysate of cells overexpressing *Shewanella oneidensis* HydE, HydF and HydG, and necessary small molecules. Briefly, apo-*Cr*HydA1 was expressed in a recombinant *E. coli* BL21(DE3) Δ*iscR* strain that harbors the plasmid containing codon-optimized *Chlamydomonas reinhardtii*

hydA1 gene with an N-terminal Strep-II purification tag. Four liters of *E. coli* cells were grown in 25 g/L LB medium with 40 mg/L kanamycin, 100 mg/L ampicillin, 2 mM ammonium ferric citrate, 0.5% (w/v) glucose and 100 mM 3-(N-morpholino)propanesulfonic acid (MOPS, pH = 7.8), at 30 °C to a OD_{600} of ~0.5, at which point the cultures were pooled, transferred into the anaerobic chamber, and supplemented with 5 mM Cys and 10 mM fumarate. The pooled culture was stirred in the chamber for 30 min to deplete the remaining oxygen in the solution and protein expression was then induced by 0.25 mM isopropyl β-D-1-thiogalactopyranoside (IPTG). After 20 h, cells were harvest by centrifugation and frozen. For protein purification, cells were lysed in a HEPES buffer (buffer A, 50 mM HEPES, 150 mM KCl, pH = 8.0, with 1 mM freshly made sodium dithionite added) containing 1xBugbuster detergent solution (EMD Millipore), 25 U/mL benzonanse (EMD Millipore), 1 kU/mL rLysozyme (EMD Millipore) and one EDTA-free protease inhibitor cocktail tablet (Roche). After the removal of cell debris by centrifugation, the clear supernatant was loaded to Strep-Tacin resin (~ 50 mL resin) in a gravity column. The column was washed with buffer A and then *Cr*HydA1 was eluted by buffer A containing 3 mM desthiobiotin. The dark fractions were collected, concentrated as necessary and stored at −80 °C.

To make cell lysate containing untagged HydE, HydF or HydG, recombinant *E. coli* cells containing the corresponding plasmid were grown and lysed (~3 mL buffer A per gram of cell) same as above. Clear cell lysate was aliquoted and stored at −80 °C. Expression levels of the maturation enzymes in the cell lysate were examined by SDS-PAGE. Desthiobiotin in the apo-*Cr*HydA1, introduced in protein purification, was removed by using a PD-10 desalting column (GE Healthcare) prior to the maturation reaction. For the maturation of *Cr*HydA1, each 25 mL reaction contained 12.5 mL HydG lysate, 4 mL HydF lysate, 1.5 mL HydE lysate, 4 mM DTT, 1 mM Fe^{2+} ($^{57}Fe^{2+}$ if necessary), 0.5 mM Na_2S, 2 mM *S*-adenosylmethionine (SAM), 2 mM Cys, 1 mM pyridoxal phosphate (PLP), 20 mM guanosine triphosphate (GTP), 2 mM tyrosine (Tyr, labeled as desired), 2 mM sodium dithionite and ~8 μM apo-*Cr*HydA1 (added in that order). The pH of the reaction mixture was adjusted to ~7.5 before dithionite was added. The reaction mixture was incubated at room temperature in an anaerobic chamber containing 2% H_2 for ~16 h, and then clarified by centrifugation. Maturated *Cr*HydA1 was re-purified from the supernatant as abovementioned (~5 mL Strep-Tactin resin). Fractions containing *Cr*HydA1 were pooled and concentrated as necessary.

Purification of uniformly ^{57}Fe-enriched *Cr*HydA1.

This procedure is same as reported in the previous study.[29] Briefly, [6^{57}Fe]-*Cr*HydA1 (that harbors the maturated H-cluster with all six iron labeled) was expressed in a recombinant *E. coli* BL21(DE3) Δ*iscR* strain that harbors two plasmids, encoding the *Chlamydomonas reinhardtii hydA1* gene and *Shewanella oneidensis hydEFGX* genes, respectively. Cell growth and protein purification were performed same as above, except that the LB media was supplemented with ^{57}Fe instead of natural abundance Fe.

EPR sample preparation.

EPR samples were made from freshly purified or maturated holo-*Ch*HydA1. To make H_{ox} samples, 2 mM thionine was added to ~ 500 μM *Ch*HydA1. The solution was immediately transferred into the EPR tube and frozen for storage. To make H_{hyd} samples, 300 mM dithionite made in buffer A was added to ~ 500 μM *Ch*HydA1.[16] The mixture was immediately transferred into the EPR tube and frozen for storage.

EPR spectroscopy.

EPR spectroscopy was performed in the CalEPR center in Department of Chemistry, University of California at Davis. X-band (9.4 GHz) Continuous Wave (CW) EPR spectra were recorded on a Bruker Biospin EleXsys E500 spectrometer equipped with a super high Q resonator (ER4122SHQE). Cryogenic temperatures were achieved and controlled by using an ESR900 liquid helium cryostat, a temperature controller (Oxford Instrument ITC503) and a gas flow controller. All CW EPR spectra were recorded at slow-passage, non-saturating conditions. Spectrometer settings were: conversion time, 40 ms; modulation amplitude, 0.5 mT; modulation frequency, 100 kHz; and other settings given in figure captions. Pulse Q-band (34 GHz) hyperfine sublevel correlation (HYSCORE) and electron nuclear double resonance (ENDOR) experiments were performed on the Bruker Biospin EleXsys 580 spectrometer using a R.A. Isaacson cylindrical TE_{011} resonator.[40] Cryogenic temperatures were achieved and controlled with an Oxford Instrument CF935 cryostat. The pulse sequences employed were as follows: free induction decay (FID)-detected field swept EPR (π/2-FID), electron spin-echo detected field swept EPR (π/2-τ-π-τ-echo), HYSCORE (π/2-τ-π/2-t1-π-t2-π/2-τ-echo), Davies-ENDOR (π-RF-π/2-τ-π-τ-echo), and Mims-ENDOR (π/2-τ-π/2-RF-π/2-τ-echo). HYSCORE time domain data were baseline corrected with 3rd polynomial, hamming-window applied, zero-filled to eight-fold of data points and fast Fourier-transformed to obtain the frequency domain results. Simulations of CW and pulse EPR spectra were performed in Matlab 2014a (MathWorks, Inc,) with EasySpin 5.2.13 toolbox.[41] Euler angles are from A tensors to g tensors and follow *z-y-z* convention.

Orientationally disordered radical systems usually exhibit anisotropic hyperfine coupling interaction (HFI) that can be decomposed into an isotropic component, a_{iso} and an anisotropic component, T. At specific orientations and for nuclei with nuclear spin $I = 1/2$ (^{13}C and ^{57}Fe in this study), the ENDOR transitions for the $m_s = \pm 1/2$ electron manifolds are observed, to first order approximation, at frequencies: $\nu\pm = |\nu_N \pm A/2|$, where ν_N is the nuclear Larmor frequency and A is the orientation-dependent hyperfine coupling.[42] In the weak coupling case where $\nu_N > A/2$, the two ENDOR peaks are centered at ν_N, and split by A. In the strong coupling case where $\nu_N > A/2$, the two ENDOR peaks are centered at $A/2$, and split by $2\nu_N$. M ims-ENDOR[43] can be used to detect very small A with superb sensitivity, but its response intensity is modulated by a factor related to A and the time interval between the first and the second microwave pulse (τ): $R \sim [1\text{-}\cos(2\pi A\tau)]$. Therefore, the intensity of Mims-ENDOR vanishes at $A = n/\tau$ ($n = 0, 1, 2 \ldots$), known as the "Mims-holes". As such, larger hyperfine couplings are typically probed by Davies-ENDOR.[43]

HYSCORE spectroscopy detects the modulation of an electron spin-echo by the spin flipping of nearby magnetic nuclei.[43] The two-dimensional spectra reveal crosspeaks, the positions of which rely on A and ν_N. For an $S = 1/2$ and $I = 1/2$ system and in the weak coupling case, the crosspeaks appear in the first quadrant at ($\nu_N + A/2$, $\nu_N - A/2$) and ($\nu_N - A/2$, $\nu_N + A/2$). In the strong coupling case, the crosspeaks appear in the second quadrant at ($\nu_N - A/2$, $\nu_N + A/2$) and ($-\nu_N - A/2$, $-\nu_N + A/2$). For HFI with large anisotropy, empirical analysis using these simple formula is not straightforward, and spectral simulation is necessary to extract the HFI parameters.

Results and discussion

[^{13}CO] in H_{ox}.

We previously reported the ^{13}C HFI of the two $^{13}CN^-$ ligands in the *Clostridium pasteurianum* hydrogenase (CpI) in the H_{ox} and H_{ox}-CO states,[25] and here we turn our focus to the three CO ligands. The CO and CN^- ligands in the H-cluster are sourced from Tyr which is cleaved by the enzyme HydG.[33, 44] In order to make ^{13}CO-specifically labeled *Cr*HydA1, we used 1-^{13}C-Tyr in the *in vitro* maturation reaction that generates the ^{13}CO ligands to the H-cluster. The maturated *Cr*HydA1 poised in the H_{ox} state was examined by CW EPR (Figure 1A), which revealed a rhombic g-tensor of [2.103, 2.042, 1.998], consistent with published results for *Cr*HydA1.[45] A small amount of H_{ox}-CO contamination (17%, g = [2.056, 2.008, 2.008]) is also present, as is often observed in [FeFe] hydrogenase samples.[45] The observed ~1 mT splitting at the three principal g values indicates a large HFI from ^{13}CO, which is similar to the observation in CpI [^{13}CN]-H_{ox}.[25] The ^{13}C HFI were further analyzed by the field-dependent Q-band Davies-ENDOR spectra recorded at the field positions without the contribution from H_{ox}-CO. We observed a total of three sets of ^{13}C ENDOR signals corresponding to the three ^{13}CO ligands in H_{ox} (Figure 1B). In line with the previous study on the HFI of the $^{13}CN^-$ ligands and the established electronic structure of H_{ox},[11–12] we assigned the ^{13}C ENDOR signal with the largest HFI, a_{iso} = 25.5 MHz (Figure 1B, green shade), to the distal ^{13}CO ($^{13}CO_d$), the ^{13}C ENDOR signal with the smallest HFI, a_{iso} = 4.5 MHz (Figure 1B, blue shade), to the proximal ^{13}CO ($^{13}CO_p$), leaving the remaining ^{13}C ENDOR signal with an HFI in-between, a_{iso} = 5.8 MHz (Figure 1B, red shade), that must arise from the bridging ^{13}CO ($^{13}CO_{bridge}$). Notably, the ^{13}C HFI of $^{13}CO_d$ is close to the cancellation limit, $A \sim 2\nu_c$, and only the higher frequency ENDOR transition is detected as the lower frequency one is close to zero and is best observed with Q-band HYSCORE spectra (Figure S1). The complex ENDOR lineshape of the higher frequency transition in the center field positions are due to narrow orientation selection of this relatively anisotropic HFI. The ^{13}C HFI of the other two ^{13}CO ligands are also confirmed by X-band HYSCORE spectroscopy (Figure S1).

The ^{13}C HFI of $^{13}CO_p$ and $^{13}CO_d$ both have magnitudes and degrees of anisotropy similar to those of the $^{13}CN_p$ and $^{13}CN_d$ ligand in CpI H_{ox}, which is consistent with the proposed local z-axis assignment of both Fe as pointing approximately along each Fe-CO_{bridge} bond.[21, 25] The a_{iso} ($^{13}CO_d$) : a_{iso} ($^{13}CO_p$) ratio of 5.7 is essentially the same with the value determined for the $^{13}CN^-$ ligands in CpI H_{ox} (5.8).[25] These findings support our previous electronic structure descriptions of H_{ox}; namely, that most spin density is carried by Fe_d and localized

in the d_z^2 orbital of this low spin $3d^7$ Fe^I.[25] The ^{13}C HFI of $^{13}CO_{bridge}$ is more dipolar, with a degree of anisotropy similar to that of $^{13}CO_{bridge}$ in DdH H_{ox}-CO, although the latter has a slightly larger a_{iso} (7.4 MHz).[24] The relatively small and anisotropic ^{13}C HFI of the $^{13}CO_{bridge}$ reflects the longer Fe-CO_{bridge} distance compared to Fe-CO_d (PDB ID: 3C8Y[3]), which diminishes the Fermi contact of the lobe of the spin-carrying Fe_d $3d_z^2$ with the ^{13}C nucleus.

In another hydrogenase sample that has higher H_{ox}-CO percentage (80%), we were able to observe four ^{13}C ENDOR signals on the Davies-ENDOR spectra recorded at $g = 2.008$ (Figure S2), $g2$ of H_{ox}-CO, with HFI values of 4.8, 7.3, 10.9 and 21.1 MHz, corresponding to the distal, proximal, bridging, and external ^{13}CO, respectively. These values are assigned by comparing to the ^{13}CO HFI values found in DdH and CpI H_{ox}-^{13}CO and the $^{13}CN^-$ HFI values found in CpI H_{ox}-CO.[24–26] The HFI values we found are in good agreement with previous results. The ^{13}C HFI values and tensors for diatomic ligands in different states of the H-cluster are summarized in Table 1.

[^{13}CO] and [^{13}CN] in H_{hyd}.

Following the published procedures to reduce *Cr*HydA1 H_{ox} with high concentration of dithionite,[14–16] we were able to readily generate *Cr*HydA1 H_{hyd}. The Q-band echo-detected EPR spectrum of the resulting sample reveals an $S = 1/2$ species with $g = [2.076, 1.936, 1.881]$ (Figure 2A), identical to the reported g values of H_{hyd} generated from wild-type *Cr*HydA1.[16] A small amount of H_{ox}-CO is also present.[15] Since both Fe_p and Fe_d in H_{hyd} are proposed to be low-spin diamagnetic Fe^{2+},[16] the ^{13}C HFI of their diatomic ligands are expected to be small. Indeed, we observed small ^{13}C HFI on the Mims-ENDOR spectra collected across the EPR absorption envelope of the [^{13}CO]-H_{hyd} sample (Figure 2B). Two sets of splittings, centered at the Larmor frequency of ^{13}C and separated by 0.2–0.5 MHz, were observed at most field positions. To clarify whether they arise from one or two ^{13}C HFI tensors, we also performed variable mixing time (VMT) Mims-ENDOR experiments which measure the absolute signs of the HFI tensors.[46] The VMT Mims-ENDOR collected at g =1.936 (Figure S3), $g2$ of H_{hyd}, indicates that the two sets of peaks do not change in the same manner as t_{mix} is increased from 1 μs to 200 μs, and they also have oppositely signed HFI. Therefore, they must correspond to two different HFI tensors. Accordingly, we simulated the field-dependent ENDOR spectra with two sets of ^{13}C HFI, with $a_{iso} = -0.16$ MHz (Figure 2B, blue shade) and −0.08 MHz (Figure 2B, red shade), respectively. Since in H_{hyd}, the spin density is proposed to localize primarily on the $[4Fe\text{-}4S]_H$ that is at +1 state, the magnitude of the small ^{13}C HFI, arising from spin polarization, would be largely governed by their distances to the $[4Fe\text{-}4S]_H$ cluster. Recent DFT calculation has also suggested that Fe_p has higher spin density than Fe_d.[18] As such, we assign the two observed ^{13}C HFI tensors to the $^{13}CO_p$ (−0.16 MHz) and $^{13}CO_{bridge}$ (−0.08 MHz) respectively (Table 1), and we reason that the ENDOR features corresponding to $^{13}CO_d$ are not observed likely because it is too distant from the unpaired electron spin leading to too small of a HFI.

To bolster this assignment, we prepared the $^{13}CN^-$-labeled *Cr*HydA1 H_{hyd} by using 2-^{13}C-Tyr as the source for the $^{13}CN^-$ ligand in the *in vitro* maturation, followed by reduction of the resulting enzyme with dithionite. In this case, the ^{13}C ENDOR signals will be less

complicated as only two $^{13}CN^-$ ligands, bound to Fe_p and Fe_d respectively, are present. Indeed, field-dependent ^{13}C Mims-ENDOR spectra of [^{13}CN]-H_{hyd} disclose only one set of ^{13}C ENDOR signals, with $|a_{iso}|$ = 0.16 MHz (Figure 2C, red trace; Table 1), the same coupling as we assigned to $^{13}CO_p$, and therefore this ^{13}C HFI can be assigned to $^{13}CN_p$. Again the ENDOR features corresponding to $^{13}CN_d$ are not observed probably due to its very small HFI.

The fact that we detected two sets of ^{13}CO but only one set of $^{13}CN^-$ indicates that the second ^{13}CO HFI must arise from the bridging, not distal, ^{13}CO. W ere this ^{13}CO to bind terminal on Fe_d, it would also have too small a HFI to be observed. The presence of a bridging CO is consistent with the FT-IR results for H_{hyd} where the observed 1857 cm^{-1} peak is within the range of observed bridging CO stretch frequency.[16] $^{13}CO/^{13}CN$ HFI results also indicate that while Fe_d is almost completely diamagnetic, Fe_p still carries a small but non-negligible amount of spin density, which may account for the isomer shift differences (~0.2 mm/s) between these two Fe centers in Mössbauer spectroscopy.[16]

Interestingly, the ^{13}C of $^{13}CN_p$ presents almost the same a_{iso} as the ^{13}C in $^{13}CO_p$ of H_{hyd}, but with a much smaller dipolar part, T, 0.05 MHz vs. 0.30 MHz. It is even smaller than that of the $^{13}CO_{bridge}$, 0.22 MHz. Since the spin density in H_{hyd} is primarily on the $[4Fe\text{-}4S]_H$ cluster, the magnitude T can be estimated accounting for the distances between each ^{13}C and the nearest Fe in the $[4Fe\text{-}4S]_H$ cluster, using the point dipole approximation and projection factors typical for $[4Fe\text{-}4S]^+$ clusters.[42, 47–49] In the X-ray crystal structure of CpI H_{ox} (PDB ID: 3C8Y[3]), such distances are 3.8 Å, 5.0Å, and 5.6 Å, for $^{13}CO_p$, $^{13}CN_p$, and $^{13}CO_{bridge}$, corresponding to T of 0.4, 0.2, and 0.15 MHz, respectively. Neglecting in this approximation possible structural rearrangements in forming H_{hyd}, it appears that the T of $^{13}CO_p$ and $^{13}CO_{bridge}$ are in agreement with the observed dipolar interactions, while the T of $^{13}CN_p$ is much smaller. The small anisotropy of $^{13}CO/^{13}CN^-$ HFI on Fe centers has been attributed to the strong covalent bonds between Fe and these π-acid ligands.[50] Upon formation of H_{hyd}, the $[2Fe]_H$ electronic configuration shifts from $Fe^{II}Fe^{I}$ to $Fe^{II}Fe^{II}$, leading to weakening of the Fe-CO bonds, as demonstrated by the increased FT-IR stretch frequencies of CO in H_{hyd} compared to H_{ox} indicating stronger C-O bonds, and with that, weaker Fe-CO bonds.[10, 16] It is therefore possible that the weaker Fe-CO bonds in H_{hyd} result in the increased rhombicity of ^{13}C HFI whereas the effects of Fe-CN bonds are much smaller.

[^{57}Fe] in H_{ox}.

The magnitudes of ^{13}CO and $^{13}CN^-$ HFI serves as reporters for the spin density of the Fe centers to which these diatomic ligands bind. In H_{ox}, however, while the $^{13}CO/^{13}CN^-$ HFI on Fe_p and Fe_d are very different (*vide supra*), previous studies on [FeFe] hydrogenases from several organisms found only one set of nearly isotropic ^{57}Fe HFI corresponding to the $[2Fe]_H$ (A ^{57}Fe = 1 2.4 or 16–18 MHz).[23, 27, 29] In an attempt to resolve this discrepancy, we sought to investigate the ^{57}Fe HFI of Fe_p and Fe_d using a combination of ENDOR and HYSCORE spectroscopies. While the molecular mechanism of the H-cluster bioassembly remains only partly understood, we found that selective installation of ^{57}Fe into the $[2Fe]_H$ subcluster can be achieved by simply supplementing 1 mM of $^{57}Fe^{2+}$ in the maturation reaction instead of natural abundance (n.a.) Fe^{2+}, using cell lysate and apo-HydA1

previously expressed with n.a. Fe-containing media. It seems likely that the $^{57}Fe^{2+}$ in the solution may reconstitute into or exchange with the somewhat labile dangler Fe site in the auxiliary cluster of HydG,[51] leading to the formation of an ^{57}Fe-labeled $Fe(CO)_2(CN)(Cys)$ product of HydG which is then incorporated in the subsequent steps of H-cluster biosynthesis.[29] We also used ^{15}N-Tyr in the reaction simply to label the CN^- ligands as $C^{15}N^-$ in order to minimize any interference from the strong ^{14}N features in HYSCORE spectra which could overlap with potential ^{57}Fe crosspeaks.

We first studied the H_{ox} state of this [2^{57}Fe]-*Cr*HydA1 compared to a uniformly ([6^{57}Fe]) ^{57}Fe-labeled sample. Q-band Davies ENDOR spectra (Figure 3A, red trace) recorded at g_1 (2.103) and g_3 (1.998) of the [2^{57}Fe] sample exhibit one major set of ^{57}Fe HFI with A = 16 MHz (Fe_A), which is consistent with the previously reported ENDOR spectra of $[2^{57}Fe]_H$-labeled *Cr*HydA H_{ox}.[29] In contrast, the spectra lack the isotropic feature with A = 10.5 MHz (Fe_B) that has been previously assigned to the $[4Fe\text{-}4S]_H$ as here seen in the ENDOR spectra (Figure 3A, blue trace) of the [6^{57}Fe]-*Cr*HydA1 H_{ox},[29] validating our selective labeling strategy. In parallel, we recorded the Q-band HYSCORE spectra of the [6^{57}Fe]- and [2^{57}Fe]-*Cr*HydA1 H_{ox} samples, which disclosed two sets of ^{57}Fe peaks in the [6^{57}Fe] sample and one set of ^{57}Fe peaks in the [2^{57}Fe] sample, both in the second quadrant and absent in a parallel sample without ^{57}Fe labeling (Figure 3B, C; Figure S4). Spectral simulation indicates that the extra ^{57}Fe peak in the [6^{57}Fe] sample, which is quite isotopic, corresponds to the Fe_B feature ($[4Fe\text{-}4S]_H$) observed in the ENDOR spectra (Figure S4). However, the ^{57}Fe peak in the [2^{57}Fe] sample, Fe_C, does not correspond to the Fe_A feature observed via ENDOR, since the HFI of the latter is much larger. The relative intensity between these Fe_B and Fe_C feature in the [6^{57}Fe] *vs.* [2^{57}Fe] sample also rules out the remote possibility that Fe_C arises from a second ^{57}Fe coupling in the small amount of the labeled $[4Fe\text{-}4S]_H$ in the [2^{57}Fe] sample. Based on these considerations, we assert that the Fe_C feature we observed in the Q-band HYSCORE spectra of the [2^{57}Fe]-*Cr*HydA1 H_{ox} sample arises from the second Fe in the $[2Fe]_H$.

The field-dependent HYSCORE spectra can be well-simulated with a rhombic ^{57}Fe HFI tensor of A = [6.5, −1.4, 12.0] MHz (a_{iso} = 5.7 MHz and T = [0.8, −7.1, 6.3] MHz, Figure 3C, Table 2). The β of 50° used in the simulation is in good agreement with the Fe_p-Fe_d-CO_{bridge} angle (44°) from the X-ray structure of the H-cluster (PDB: 3C8Y[3]), which is consistent with A_3 being along the Fe_d-Fe_p vector if we assign g_3 as pointing along the Fe_d-CO_{bridge} bonding vector (*vide infra)* No corresponding ENDOR signal could be identified for this HFI tensor (Figure S5), probably due to its large rhombicity. Since selective labeling of a single specific Fe in the $[2Fe]_H$ subcluster is not yet feasible, we cannot assign this ^{57}Fe HFI to a specific Fe. However, the relatively smaller a_{iso} suggests that this ^{57}Fe HFI may be assigned to Fe_p, with the stronger 16–18 MHz (a_{iso} ~ 17 MHz) coupling arising from Fe_d. In this case, the a_{iso} (Fe_d)/a_{iso} (Fe_p) ratio of 3.0 is more consistent with Fe_d carrying the majority spin density as inferred from ^{13}C HFI results and theoretical predictions,[21, 25, 31] although it is still approximately two-fold smaller than the a_{iso} ($^{13}CO_d$)/a_{iso} ($^{13}CO_p$) ratio (or that of the $^{13}CN^-$ ligands). This difference may be attributed to the rhombicity of the A-tensor of Fe_p, which may affect the ^{13}C HFI in a manner we have not fully accounted.

More importantly, the fact that the two Fe sites of the $[2Fe]_H$ are indeed electronically different is crucial for the catalytic activity of the [FeFe] hydrogenase. This Fe sites heterogeneity, together with the magnitudes of the hyperfine couplings, can be used as a guide for designing molecular models for [FeFe] hydrogenases. For instance, one such synthetic complex has been characterized, showing that the ^{57}Fe HFI on the two Fe sites are different by a factor of ~2 in H_{ox} models, similar to that found in the hydrogenase enzyme.[52]

[^{57}Fe] in H_{hyd}

When the [2^{57}Fe]-*Cr*HydA1 sample is poised in the H_{hyd} state, we expect to see small ^{57}Fe HFI as the ^{13}CO and $^{13}CN^-$ HFI on these Fe are very small (*vide supra*). Indeed, in the field-dependent Q-band HYSCORE spectra, we were only able to see intensity on the diagonal line at the Larmor frequency of ^{57}Fe, likely from the two overlapping ^{57}Fe HFI. The largest principal value of these ^{57}Fe HFI was estimated by the feature at $g2$ which showed a width of ~0.3 MHz. Notably, since there was a small amount of H_{ox}-CO in the H_{hyd} sample, HYSCORE spectra recorded at $g = 2.008$, $g2$ of H_{ox}-CO, showed two sets of crosspeaks in the first and the second quadrant (Figure S6), corresponding to the Fe_d and Fe_p in this [2^{57}Fe]-H_{ox}-CO, respectively. This HYSCORE patterns are identical to those of the previously reported *Cr*HydA1 H_{ox}-CO sample maturated using the synthetic $[^{57}Fe_2(CO)_4(CN)_2(adt)]^{2-}$, and can be well-simulated with the reported ^{57}Fe HFI tensors.[53] This further proves that both Fe_d and Fe_p are labeled in the sample.

The very small ^{57}Fe HFI arising from the $[2Fe]_H$ supports the diamagnetic low-spin Fe^{2+} assignment of these two Fe sites. The ^{57}Fe HFI of the remaining paramagnetic $[4Fe\text{-}4S]_H^+$ was then measured using the uniformly ^{57}Fe-labeled H_{hyd} sample generated by reducing the [6^{57}Fe]-*Cr*HydA1 with dithionite. The X-band CW EPR of the [6^{57}Fe]-*Cr*HydA1 H_{hyd}, but not the [2^{57}Fe]-H_{hyd}, shows line broadening at g_3 (Figure S7), indicating the presence of large ^{57}Fe HFI from the $[4Fe\text{-}4S]_H$ of H_{hyd}, as expected. The Q-band field-dependent Davies ENDOR spectra further reveal these large ^{57}Fe couplings (Fe_1 and Fe_2, Figure 5A), and are simulated with two sets of ^{57}Fe HFI, with a_{iso} of 28.2 MHz and 35.3 MHz, respectively (Table 2). These ^{57}Fe hyperfine values are similar to that of the mixed-valance $Fe^{2.5+}$ pair found in typical $[4Fe\text{-}4S]^+$ clusters.[48] More interestingly, additional ^{57}Fe HFI are disclosed by Q-band HYSCORE spectroscopy, as indicated from the crosspeaks in the second quadrant of the HYSCORE spectra collected at $g = 1.881$, g_3 of H_{hyd} (Fe_3 and Fe_4, Figure 5B). Simulation of the field-dependent HYSCORE spectra (Figure 5B and S8) gives two ^{57}Fe HFI tensors, a rhombic one with a_{iso} of 7.5 MHz (Figure 5B and S8, blue contours) and an axial one with a_{iso} of 16.6 MHz (Figure 5B and S8, green contours), corresponding to the two remaining Fe^{2+} in the $[4Fe\text{-}4S]_H$ (Table 2). The a_{iso} of 16.6 MHz is comparable to typical ^{57}Fe HFI of ferrous pair (Fe^{2+}) found in the $[4Fe\text{-}4S]^+$ clusters of various ferredoxins and synthetic systems, whereas the a_{iso} of 7.2 MHz is much smaller than these typical values.[48] It has been noted in aconitase that the unique substrate-binding Fe has the smallest ^{57}Fe HFI among the four Fe.[48, 54] It is likely that in H_{hyd}, this small ^{57}Fe HFI also arises from the unique Fe^{2+} that is coordinated by the bridging Cys residue by which the $[4Fe\text{-}4S]_H$ is linked to the $[2Fe]_H$. Together, these ^{57}Fe HFI results depict the electronic structure of $[4Fe\text{-}4S]_H$ in H_{hyd} as having antiferromagnetically coupled $Fe^{2.5+}$ pair and Fe^{2+} pair, leading to an $S = 1/2$ subcluster. However, the presence of the $[2Fe]_H$ in close proximity

has considerably affected the electronic structure of the $[4Fe\text{-}4S]_H$, most significantly so on the unique Fe, despite the former being formally diamagnetic.

The ^{13}C and ^{57}Fe HFI results of H_{hyd} validate the electronic structural description proposed from Mössbauer spectroscopy that the $[2Fe]_H$ contains two diamagnetic low-spin Fe^{2+}.[16] The small ^{13}C and ^{57}Fe HFI in the $[2Fe]_H$ most likely arise from spin delocalization via covalency and spin polarization, and the exchange interaction to the $[4Fe\text{-}4S]_H$ is almost nil because of the much higher energy gap between the $S = 0$ and $S = 1$ states for low-spin Fe^{2+}. It is therefore safe to write H_{hyd} as $[4Fe\text{-}4S]_H^+$-$[Fe^{II}Fe^{II}]$-H^-. The diamagnetic nature of the $[2Fe]_H$ is also consistent with the recently reported ^1H NMR spectra of H_{hyd}, in which the terminal hydride has a very small, if any, paramagnetic shift.[13] As noted above, the small ^{13}C and ^{57}Fe HFI in H_{hyd} are reminiscent of that in the HydG reaction intermediate we recently characterized—the $[4Fe\text{-}4S]^+$ -[(Cys)Fe^{II}(CO)(CN)] intermediate termed "Complex A" also harbors a CO and CN^- bound low-spin Fe^{2+}.[32] But compared to Complex A, the ^{13}C and ^{57}Fe HFI are even smaller in H_{hyd}, indicating a smaller spin density on Fe_p and Fe_d in H_{hyd}. This difference could be due to a variety of factors. The nearest iron of the [4Fe-4S] could be closer to the dangler Fe in Complex A; it could have a larger spin projection value; or the Fe-S_{Cys}-Fe bond angle could be more amenable for spin delocalization via covalency.

If we view H_{hyd} as resulting from the binding of an H^- onto the Fe_d of H_{ox}, this is accompanied by the movement of one electron from the $[2Fe]_H$ to the $[4Fe\text{-}4S]_H$. This is exactly opposite to the cases of $H_{red}/H_{red}H^+$—recently identified to be $[4Fe\text{-}4S]_H^+$-$[Fe^IFe^{II}]_H$ and $[4Fe\text{-}4S]_H^{2+}$-$[Fe^IFe^I]_H$-(NH_2^+) respectively—where the protonation on the adt amine is accompanied by one electron moving from the $[4Fe\text{-}4S]_H$ to the $[2Fe]_H$.[8] It appears that the net charge on the $[2Fe]_H$ tends to remain unchanged, as implied in previous work as the "neutralization effect".[8] The $[4Fe\text{-}4S]_H$—in addition to its roles in mediating electron transfer in catalysis—could serve as an electron sink or source to facilitate electronic rearrangement during the catalytic cycle in order to maintain the overall structural integrity of the H-cluster. In this regard, further protonation of H_{hyd} on the adt amine would lead to a $H_{hyd}H^+$ state that is proposed to adopt a $[4Fe\text{-}4S]_H^{2+}$-$[Fe^{II}Fe^I]_H$-(NH_2^+)-H^- configuration and to release H_2 rapidly before returning to H_{ox}.[18] Spectroscopic characterization on this transient species would be of great interest if conditions favoring its accumulation can be found since in $H_{hyd}H^+$, the spin density is purported to be localized on the $[2Fe]_H$ again, and one would expect to see the much larger ^1H HFI of the terminal hydride (or H_2 molecule) bound to Fe_d directly by EPR/ENDOR spectroscopy.

Conclusion

The *in vitro* biosynthetic route to the H-cluster has demonstrated its convenience and versatility to site-specifically label the H-cluster with desired magnetic nuclei. This biochemical approach, combined with advanced EPR spectroscopic techniques, allow us to study the electronic structure of the H-cluster at two catalytic states, H_{ox} and H_{hyd}. For H_{ox}, we measured the ^{13}C HFI of the three ^{13}CO ligands, which is a natural outgrowth of our previous work on the two $^{13}CN^-$ ligands. We re-investigated the ^{57}Fe HFI of the $[2Fe]_H$, and identified for the first time a second set of ^{57}Fe HFI. This work shows that the two Fe in the $[2Fe]_H$ have different HFI, which agrees with the results from the spectroscopic study of the

$^{13}CO/^{13}CN$ ligands on these Fe sites, and largely solves a controversy from previous spectroscopic and theoretical studies. For H_{hyd}, we detected very small ^{13}C and ^{57}Fe HFI in the $[2Fe]_H$ subcluster, and four much larger ^{57}Fe HFI in the $[4Fe\text{-}4S]_H$ subcluster, consistent with the proposed electronic structural description of H_{hyd} as $[4Fe\text{-}4S]_H^+[Fe^{II}Fe^{II}]\text{-}H^-$. Overall, our work represents a comprehensive spectroscopic investigation on the H-cluster. These results, together with the numerous recent advances with the [FeFe] hydrogenases, helps enhance our understanding on this unique cofactor, and guide *de novo* design of molecular catalysts for hydrogen evolution.

Supplementary Material

Refer to Web version on PubMed Central for supplementary material.

Acknowledgment

We thank J. Swartz (Stanford) for providing *E. coli* strains overexpressing apo-*Cr*HydA1, holo-*Cr*HydA1, *So*HydE, *So*HydF and *So*HydG, D.L.M. Suess and R. Sayler for preliminary ENDOR results on $[^{13}CO]$-CpI H_{ox}, W. Myers for initial spectroscopic results on [Fe]-HydA1 H_{ox}, and T. Stich for helpful discussions and proofreading the manuscript. This work was supported by the National Institutes of Health (GM-104543 and 1R35GM126961–01).

References

1. Lubitz W; Ogata H; Rudiger O; Reijerse E, Hydrogenases. Chem. Rev 2014, 114 (8), 4081–148. [PubMed: 24655035]
2. Vignais PM; Billoud B, Occurrence, classification, and biological function of hydrogenases: an overview. Chem. Rev 2007, 107 (10), 4206–72. [PubMed: 17927159]
3. Pandey AS; Harris TV; Giles LJ; Peters JW; Szilagyi RK, Dithiomethylether as a ligand in the hydrogenase H-cluster. J. Am. Chem Soc 2008, 130 (13), 4533–40. [PubMed: 18324814]
4. Peters JW; Lanzilotta WN; Lemon BJ; Seefeldt LC, X-ray crystal structure of the Fe- only hydrogenase (CpI) from Clostridium pasteurianum to 1.8 angstrom resolution. Science 1998, 282 (5395), 1853–8. [PubMed: 9836629]
5. Nicolet Y; Piras C; Legrand P; Hatchikian CE; Fontecilla-Camps JC, Desulfovibrio desulfuricans iron hydrogenase: the structure shows unusual coordination to an active site Fe binuclear center. Structure 1999, 7 (1), 13–23. [PubMed: 10368269]
6. Silakov A; Wenk B; Reijerse E; Lubitz W, ^{14}N HYSCORE investigation of the H-cluster of [FeFe] hydrogenase: evidence for a nitrogen in the dithiol bridge. Phys. Chem. Chem. Phys 2009, 11 (31), 6592–9. [PubMed: 19639134]
7. Chongdar N; Birrell JA; Pawlak K; Sommer C; Reijerse EJ; Rudiger O; Lubitz W; Ogata H, Unique spectroscopic properties of the H-cluster in a putative sensory [FeFe] hydrogenase. J. Am. Chem. Soc 2018, 140 (3), 1057–1068. [PubMed: 29251926]
8. Sommer C; Adamska-Venkatesh A; Pawlak K; Birrell JA; Rüdiger O; Reijerse EJ; Lubitz W, Proton coupled electronic rearrangement within the H-cluster as an essential step in the catalytic cycle of [FeFe] hydrogenases. J. Am. Chem. Soc 2017, 139 (4), 1440–1443. [PubMed: 28075576]
9. Adamska-Venkatesh A; Krawietz D; Siebel J; Weber K; Happe T; Reijerse E; Lubitz W, New redox states observed in [FeFe] hydrogenases reveal redox coupling within the H-cluster. J. Am. Chem. Soc 2014, 136 (32), 11339–46. [PubMed: 25025613]
10. Adamska A; Silakov A; Lambertz C; Rüdiger O; Happe T; Reijerse E; Lubitz W, Identification and characterization of the “super-reduced” state of the H-cluster in [FeFe] hydrogenase: A new building block for the catalytic cycle? Angew. Chem. Int. Ed 2012, 51 (46), 11458–11462.
11. Katz S; Noth J; Horch M; Shafaat HS; Happe T; Hildebrandt P; Zebger I, Vibrational spectroscopy reveals the initial steps of biological hydrogen evolution. Chem Sci. 2016, 7 (11), 6746–6752. [PubMed: 28451119]

12. Popescu CV; Münck E, Electronic structure of the H cluster in [Fe]-hydrogenases. J. Am. Chem. Soc 1999, 121 (34), 7877–7884.

13. Rumpel S; Sommer C; Reijerse E; Fares C; Lubitz W, Direct detection of the terminal hydride intermediate in [FeFe] hydrogenase by NMR spectroscopy. J. Am. Chem Soc 2018.

14. Winkler M; Senger M; Duan J; Esselborn J; Wittkamp F; Hofmann E; Apfel UP; Stripp ST; Happe T, Accumulating the hydride state in the catalytic cycle of [FeFe]-hydrogenases. Nat Commun 2017, 8, 16115. [PubMed: 28722011]

15. Reijerse EJ; Pham CC; Pelmenschikov V; Gilbert-Wilson R; Adamska-Venkatesh A; Siebel JF; Gee LB; Yoda Y; Tamasaku K; Lubitz W; Rauchfuss TB; Cramer SP, Direct observation of an iron-bound terminal hydride in [FeFe]-hydrogenase by nuclear resonance vibrational spectroscopy. J. Am. Chem. Soc 2017, 139 (12), 4306–4309. [PubMed: 28291336]

16. Mulder DW; Guo Y; Ratzloff MW; King PW, Identification of a catalytic iron-hydride at the H-cluster of [FeFe]-hydrogenase. J. Am. Chem. Soc 2017, 139 (1), 83–86. [PubMed: 27973768]

17. Mulder DW; Ratzloff MW; Bruschi M; Greco C; Koonce E; Peters JW; King PW, Investigations on the role of proton-coupled electron transfer in hydrogen activation by [FeFe]-hydrogenase. J. Am. Chem. Soc 2014, 136 (43), 15394–15402. [PubMed: 25286239]

18. Pelmenschikov V; Birrell JA; Pham CC; Mishra N; Wang H; Sommer C; Reijerse E; Richers CP; Tamasaku K; Yoda Y; Rauchfuss TB; Lubitz W; Cramer SP, Reaction coordinate leading to H_2 production in [FeFe]-hydrogenase Iidentified by nuclear resonance vibrational spectroscopy and density functional theory. J. Am. Chem. Soc 2017, 139 (46), 16894–16902. [PubMed: 29054130]

19. Carroll ME; Barton BE; Rauchfuss TB; Carroll PJ, Synthetic models for the active site of the [FeFe]-hydrogenase: Catalytic proton reduction and the structure of the doubly protonated intermediate. J. Am. Chem. Soc 2012, 134 (45), 18843–18852. [PubMed: 23126330]

20. Kalz KF; Brinkmeier A; Dechert S; Mata RA; Meyer F, Functional model for the [Fe] hydrogenase inspired by the frustrated lewis pair concept. J. Am. Chem Soc 2014, 136 (47), 16626–16634. [PubMed: 25353322]

21. Fiedler AT; Brunold TC, Computational studies of the H-cluster of Fe-only hydrogenases: Geometric, electronic, and magnetic properties and their dependence on the [Fe4S4] cubane. Inorg. Chem 2005, 44 (25), 9322–9334. [PubMed: 16323916]

22. Silakov A; Reijerse EJ; Lubitz W, Unraveling the electronic properties of the photoinduced states of the H - cluster in the [FeFe] hydrogenase from D. desulfuricans. Eur. J. Inorg. Chem 2011, 2011 (7), 1056–1066.

23. Silakov A; Reijerse EJ; Albracht SPJ; Hatchikian EC; Lubitz W, The electronic structure of the H-cluster in the [FeFe]-hydrogenase from Desulfovibrio desulfuricans: A Q-band ^{57}Fe-ENDOR and HYSCORE study. J. Am. Chem. Soc 2007, 129 (37), 11447–11458. [PubMed: 17722921]

24. Silakov A; Wenk B; Reijerse E; Albracht SP; Lubitz W, Spin distribution of the H-cluster in the H_{ox}-CO state of the [FeFe] hydrogenase from Desulfovibrio desulfuricans: HYSCORE and ENDOR study of ^{14}N and ^{13}C nuclear interactions. J. Biol. Inorg. Chem 2009, 14 (2), 301–13. [PubMed: 19011912]

25. Myers WK; Stich TA; Suess DLM; Kuchenreuther JM; Swartz JR; Britt RD, The cyanide ligands of [FeFe] hydrogenase: Pulse EPR studies of ^{13}C and ^{15}N-labeled H-cluster. J. Am. Chem. Soc 2014, 136 (35), 12237–12240. [PubMed: 25133957]

26. Telser J; Benecky MJ; Adams MW; Mortenson LE; Hoffman BM, An EPR and electron nuclear double resonance investigation of carbon monoxide binding to hydrogenase I (bidirectional) from Clostridium pasteurianum W5. J. Biol. Chem 1986, 261 (29), 13536–41. [PubMed: 3020036]

27. Wang G; Benecky MJ; Huynh BH; Cline JF; Adams MW; Mortenson LE; Hoffman BM; Munck E, Mossbauer and electron nuclear double resonance study of oxidized bidirectional hydrogenase from Clostridium pasteurianum W5. J. Biol. Chem 1984, 259 (23), 14328–31. [PubMed: 6094552]

28. Rumpel S; Ravera E; Sommer C; Reijerse E; Fares C; Luchinat C; Lubitz W, ^{1}H NMR spectroscopy of [FeFe] hydrogenase: Insight into the electronic structure of the active site. J. Am. Chem. Soc 2018, 140 (1), 131–134. [PubMed: 29211457]

29. Kuchenreuther JM; Myers WK; Suess DL; Stich TA; Pelmenschikov V; Shiigi SA; Cramer SP; Swartz JR; Britt RD; George SJ, The HydG enzyme generates an Fe(CO)2(CN) synthon in

assembly of the FeFe hydrogenase H-cluster. Science 2014, 343 (6169), 424–7. [PubMed: 24458644]

30. Silakov A; Reijerse EJ; Albracht SP; Hatchikian EC; Lubitz W, The electronic structure of the H-cluster in the [FeFe]-hydrogenase from Desulfovibrio desulfuricans: a Q-band ^{57}Fe-ENDOR and HYSCORE study. J. Am. Chem. Soc 2007, 129 (37), 11447–58. [PubMed: 17722921]
31. Greco C; Silakov A; Bruschi M; Ryde U; Gioia LD; Lubitz W, Magnetic properties of [FeFe] -hydrogenases: A theoretical investigation based on extended QM and QM/MM models of the H -cluster and its surroundings. Eur. J. Inorg. Chem 2011, 2011 (7), 1043–1049.
32. Rao G; Tao L; Suess DLM; Britt RD, A [4Fe-4S]-Fe(CO)(CN)-L-cysteine intermediate is the first organometallic precursor in [FeFe] hydrogenase H-cluster bioassembly. Nat. Chem 2018, 10 (5), 555–560. [PubMed: 29632334]
33. Kuchenreuther JM; Myers WK; Stich TA; George SJ; Nejatyjahromy Y; Swartz JR; Britt RD, A radical intermediate in tyrosine scission to the CO and CN^- ligands of FeFe hydrogenase. Science 2013, 342 (6157), 472–5. [PubMed: 24159045]
34. Mulder DW; Boyd ES; Sarma R; Lange RK; Endrizzi JA; Broderick JB; Peters JW, Stepwise [FeFe]-hydrogenase H-cluster assembly revealed in the structure of HydA(DeltaEFG). Nature 2010, 465 (7295), 248–51. [PubMed: 20418861]
35. Posewitz MC; King PW; Smolinski SL; Zhang L; Seibert M; Ghirardi ML, Discovery of two novel radical S-adenosylmethionine proteins required for the assembly of an active [Fe] hydrogenase. J. Biol. Chem 2004, 279 (24), 25711–20. [PubMed: 15082711]
36. Shepard EM; McGlynn SE; Bueling AL; Grady-Smith CS; George SJ; Winslow MA; Cramer SP; Peters JW; Broderick JB, Synthesis of the 2Fe subcluster of the [FeFe]-hydrogenase H cluster on the HydF scaffold. Proc. Natl. Acad. Sci. U. S. A 2010, 107 (23), 10448–53. [PubMed: 20498089]
37. Kuchenreuther JM; Shiigi SA; Swartz JR, Cell-free synthesis of the H-cluster: a model for the in vitro assembly of metalloprotein metal centers. Methods Mol. Biol 2014, 1122, 49–72. [PubMed: 24639253]
38. Boyer ME; Stapleton JA; Kuchenreuther JM; Wang CW; Swartz JR, Cell-free synthesis and maturation of [FeFe] hydrogenases. Biotechnol. Bioeng 2008, 99 (1), 59–67. [PubMed: 17546685]
39. Kuchenreuther JM; Britt RD; Swartz JR, New insights into [FeFe] hydrogenase activation and maturase function. PLoS One 2012, 7 (9), e45850.
40. Calvo R; Abresch EC; Bittl R; Feher G; Hofbauer W; Isaacson RA; Lubitz W; Okamura MY; Paddock ML, EPR study of the molecular and electronic structure of the semiquinone biradical Qa −•Qb−• in photosynthetic reaction centers from Rhodobacter sphaeroides. J. Am. Chem. Soc 2000, 122 (30), 7327–7341.
41. Stoll S; Schweiger A, EasySpin, a comprehensive software package for spectral simulation and analysis in EPR. J. Magn. Reson 2006, 178 (1), 42–55. [PubMed: 16188474]
42. Weil JA; Bolton JR, Hyperfine (A) anisotropy In Electron Paramagnetic Resonance, John Wiley & Sons, Inc.: 2006; pp 118–157.
43. Schweiger A; Jeschke G, Principles of pulse electron paramagnetic resonance. Oxford University Press: USA, 2001.
44. Kuchenreuther JM; George SJ; Grady-Smith CS; Cramer SP; Swartz JR, Cell-free H-cluster synthesis and [FeFe] hydrogenase activation: All five CO and CN− ligands derive from tyrosine. PLoS One 2011, 6 (5), e20346. [PubMed: 21673792]
45. Kamp C; Silakov A; Winkler M; Reijerse EJ; Lubitz W; Happe T, Isolation and first EPR characterization of the [FeFe]-hydrogenases from green algae. Biochim. Biophys. Acta 2008, 1777 (5), 410–6. [PubMed: 18355437]
46. Epel B; Niklas J; Antonkine ML; Lubitz W, Absolute signs of hyperfine coupling constants as determined by pulse ENDOR of polarized radical pairs. Appl. Magn. Reson 2006, 30 (3), 311–327.
47. Walsby CJ; Hong W; Broderick WE; Cheek J; Ortillo D; Broderick JB; Hoffman BM, Electron-nuclear double resonance spectroscopic evidence that S-adenosylmethionine binds in contact with the catalytically active $[4Fe\text{-}4S]^+$ cluster of pyruvate formate-lyase activating enzyme. J. Am. Chem. Soc 2002, 124 (12), 3143–3151. [PubMed: 11902903]

48. Mouesca JM; Noodleman L; Case DA; Lamotte B, Spin-densities and spin coupling in iron-sulfur clusters - a new analysis of hyperfine coupling-constants. Inorg. Chem 1995, 34 (17), 4347–4359.

49. Weil JA; Bolton JR, The interpretation of EPR parameters In Electron Paramagnetic Resonance, John Wiley & Sons, Inc.: 2006; pp 253–300.

50. Telser J; Smith ET; Adams MWW; Conover RC; Johnson MK; Hoffman BM, Cyanide binding to the novel 4Fe ferredoxin from Pyrococcus Furiosus: Investigation by EPR and ENDOR spectroscopy. J. Am. Chem. Soc 1995, 117 (18), 5133–5140.

51. Suess DL; Burstel I; De La Paz L; Kuchenreuther JM; Pham CC; Cramer SP; Swartz JR; Britt RD, Cysteine as a ligand platform in the biosynthesis of the FeFe hydrogenase H cluster. Proc. Natl. Acad. Sci. U. S. A 2015, 112 (37), 11455–60. [PubMed: 26324916]

52. Stoian SA; Hsieh CH; Singleton ML; Casuras AF; Darensbourg MY; McNeely K; Sweely K; Popescu CV, Hyperfine interactions and electron distribution in Fe(II)Fe (I) and Fe (I)Fe (I) models for the active site of the [FeFe] hydrogenases: Mossbauer spectroscopy studies of low-spin Fe(I.). J. Biol. Inorg. Chem 2013, 18 (6), 609–22. [PubMed: 23700296]

53. Gilbert-Wilson R; Siebel JF; Adamska-Venkatesh A; Pham CC; Reijerse E; Wang H; Cramer SP; Lubitz W; Rauchfuss TB, Spectroscopic investigations of [FeFe] hydrogenase maturated with [57Fe2(adt)(CN)2(CO)4]2−. J. Am. Chem. Soc 2015, 137 (28), 8998–9005. [PubMed: 26091969]

54. Werst MM; Kennedy MC; Houseman AL; Beinert H; Hoffman BM, Characterization of the [4Fe-4S]+ cluster at the active site of aconitase by 57Fe, 33S, and 14N electron nuclear double resonance spectroscopy. Biochemistry 1990, 29 (46), 10533–40. [PubMed: 2271662]

Synopsis:

The electronic structures of the two catalytic states of the [FeFe] hydrogenase H-cluster, H_{ox} and H_{hyd}, are studied by probing the hyperfine couplings of the ^{13}C and ^{57}Fe nuclei in site-specific isomiddlee-labeled H-cluster. For H_{ox}, two different ^{57}Fe hyperfine interactions are observed for the two Fe sites of the spin-carrying $[2Fe]_H$ subcluster. For H_{hyd}, the weakly coupled ^{13}C and ^{57}Fe are detected, consistent with previous description of this newly identified form of H-cluster.

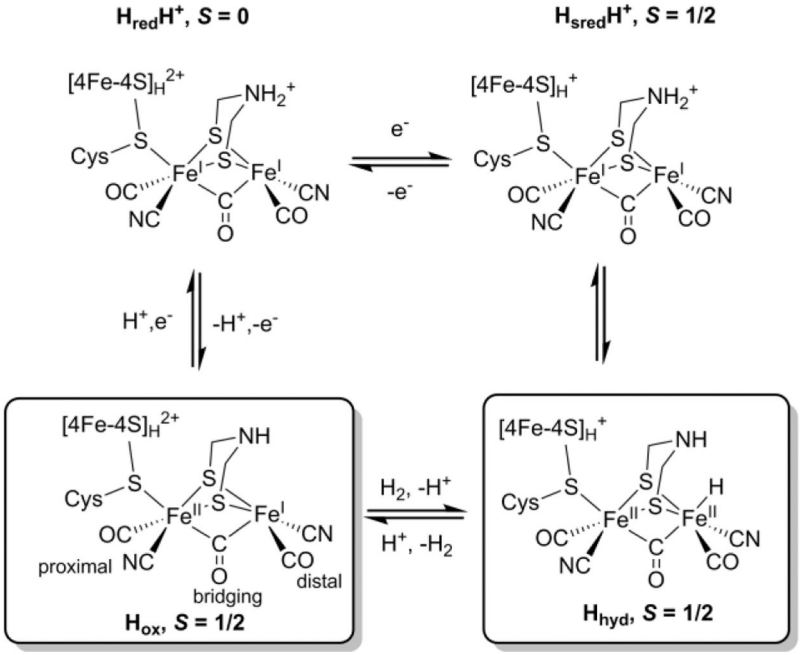

Scheme 1.

Proposed catalytic cycle of the H-cluster highlighting the two $S = 1/2$ states, H_{ox} and H_{hyd}.

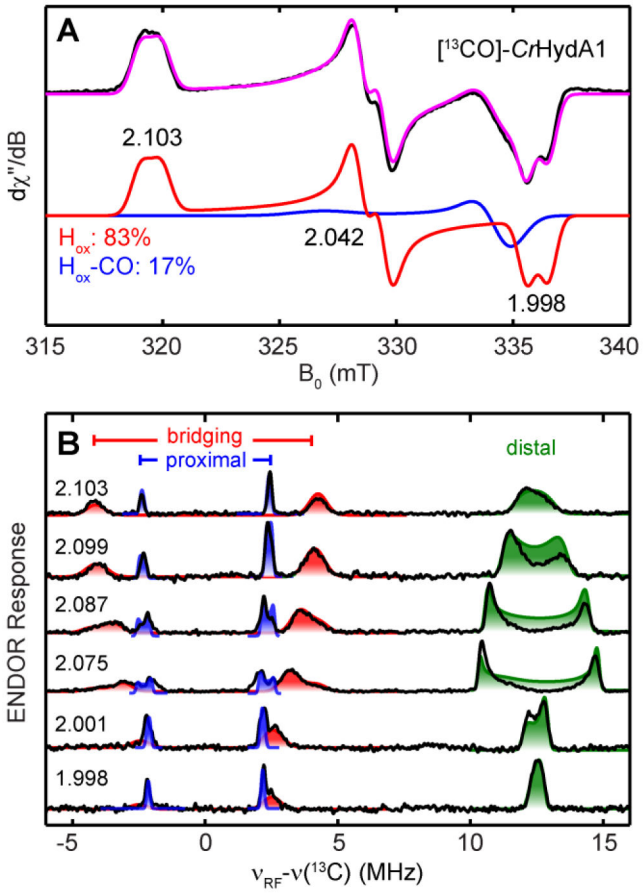

Figure 1.

(**A**) X-band CW EPR spectrum of thionine-oxidized [^{13}CO]-*Cr*HydA1 (black trace) and the total simulation (magenta trace). The two spectral components are: H_{ox}, g = [2.103, 2.042, 1.998], 83% (red trace); H_{ox}-CO, g = [2.056, 2.008, 2.008], 17% (blue trace). Conditions: frequency, 9.4 GHz; temperature, 15 K; microwave power, 4 μW. (**B**) Q-band field-dependent Davies-ENDOR spectra (black trace) of [^{13}CO]-*Cr*HydA1 H_{ox} simulated with three sets of ^{13}C HFI. Simulation: g = [2.103, 2.042, 1.998]; $^{13}CO_d$ (green shade): A = [20.5, 29.9, 26.0] MHz, Euler angle = [37, 26, 0]°; $^{13}CO_p$ (blue shade): A = [5.3, 4.0, 4.3] MHz, Euler angle = [25, 25, 0]°; $^{13}CO_{bridge}$ (red shade): A = [9.0, 3.8, 4.5] MHz, Euler angle = [0, 20, 0]°. Conditions: frequency, 34.1 GHz; temperature, 15K; inversion pulse, 80 ns; RF pulse, 30 μs; **π**/2, 12ns; **τ** = 300 ns.

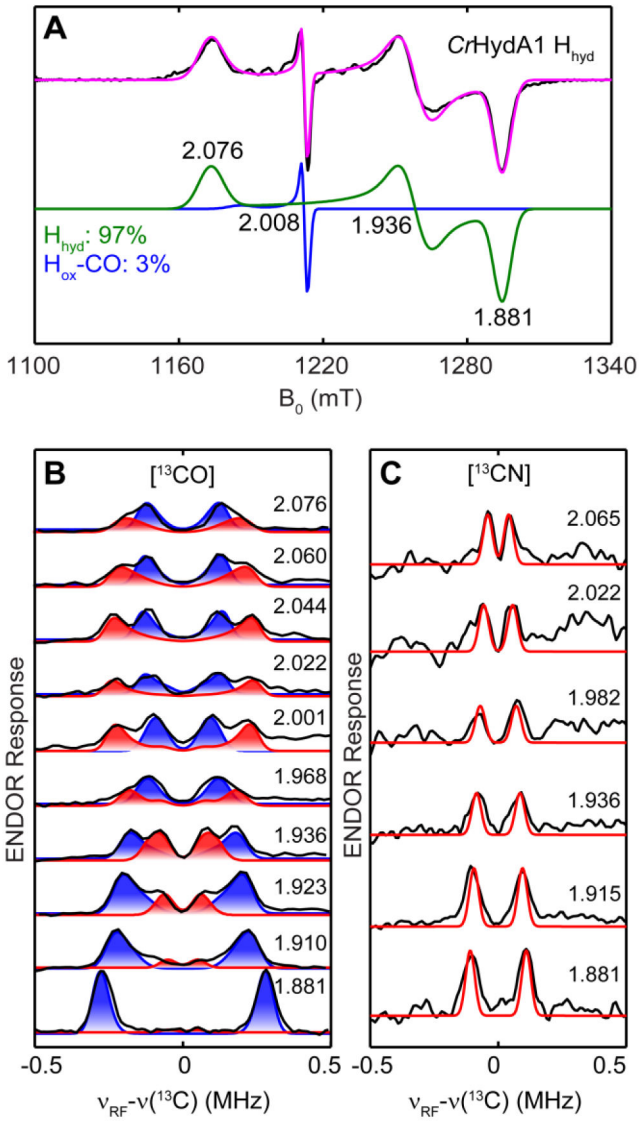

Figure 2.

(**A**) Pseudo-modulated Q-band echo-detected EPR spectrum of dithionite-reduced *Cr*HydA1 (black trace) and the total simulation (magenta trace). The two spectral components are: H_{hyd}, g = [2.076, 1.936, 1.881], 97% (green trace); H_{ox}-CO, g = [2.056, 2.008, 2.008], 3% (blue trace). Conditions: frequency, 34.1 GHz; temperature, 10 K; τ = 300 ns; modulation amplitude, 0.5 mT. (**B, C**) Q-band field-dependent Mims-ENDOR spectra (black trace) of [^{13}CO]-*Cr*HydA1 H_{hyd} simulated with two sets of ^{13}C HFI (**B**), and that of [^{13}CN]-*Cr*HydA1 H_{hyd} simulated with one ^{13}C HFI (**C**). Simulation: g = [2.076, 1.936, 1.881]; $^{13}CO_p$ (blue shade): A = [0.30, −0.18, −0.59] MHz, Euler angle = [25, 0, 0]°; $^{13}CO_{bridge}$ (red shade): A = [−0.51, 0.16, 0.10] MHz, Euler angle = [35, 0, 0]°; $^{13}CN_p$ (red trace): A = [0.07, 0.17, 0.22] MHz, Euler angle = [0, 10, 0]°. Conditions for Mims-ENDOR: frequency, 34.1 GHz; temperature, 10K; RF pulse, 30 μs; $\pi/2$, 12 ns; τ = 600 ns.

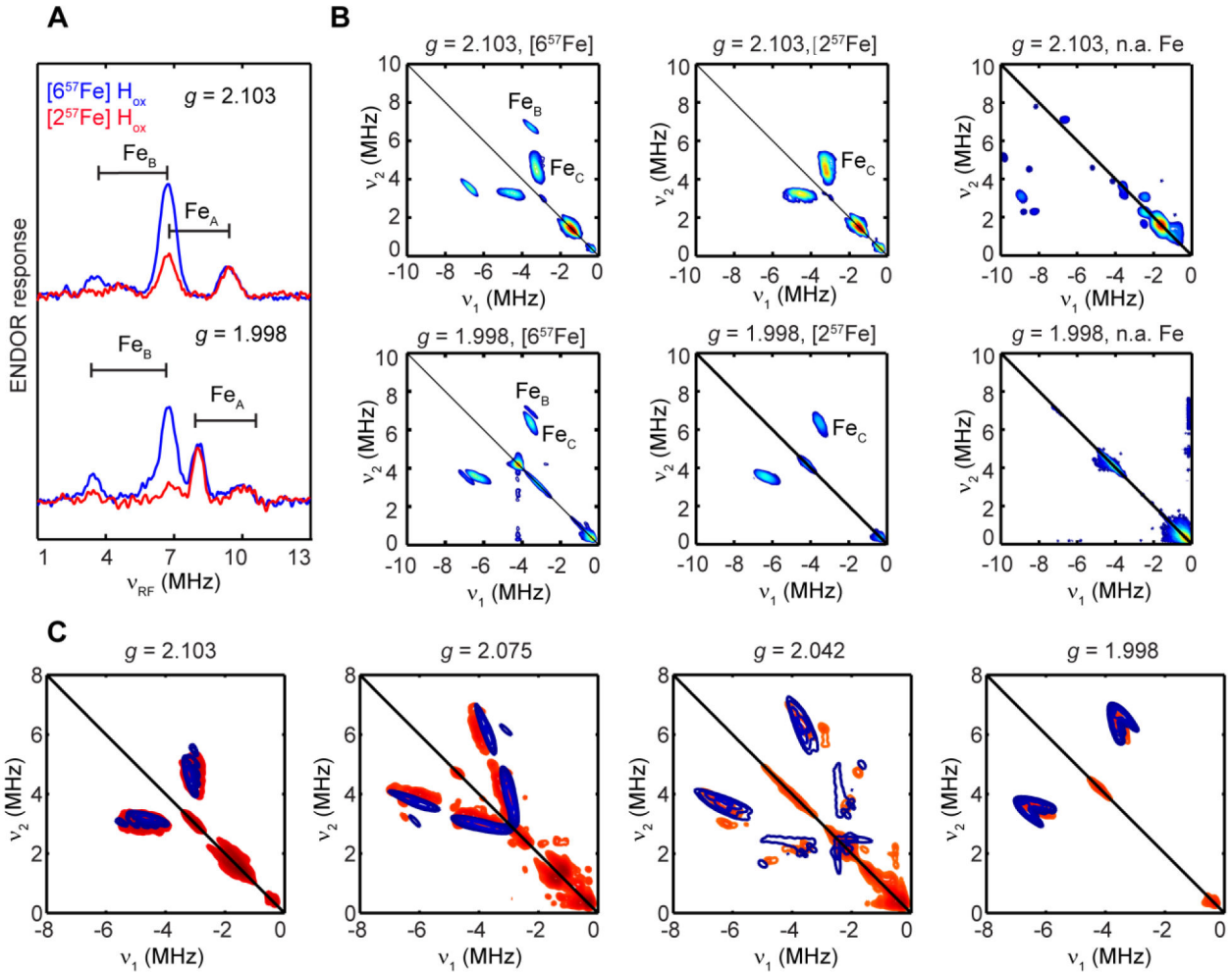

Figure 3.

(**A**) Comparison of the Q-band Davies ENDOR spectra of [2^{57}Fe]-*Ci*HydA1 H_{ox} (red trace) and [6^{57}Fe]-*Ci*HydA1 H_{ox} (blue trace) recorded at g = 2.103 and 1.998. (**B**) Comparison of the Q-band HYSCORE spectra of [6^{57}Fe]- (left panels), [2^{57}Fe]-(middle panels), and n.a. Fe (right panels) *Ci*HydA1 H_{ox} samples recorded at g = 2.103 and 1.998 showing the ^{57}Fe peaks in the second quadrant. (**C**) Field-dependent Q-band ^{57}Fe HYSCORE spectra of the [2^{57}Fe]-*Ci*HydA1 H_{ox} sample (red contours) and simulations of Fe_C (blue contours). Simulation: g = [2.103, 2.042, 1.998], A $^{57}Fe_C$ = [6.5, −1.4, 12.0] MHz, Euler angle = [17, 50, 25]° Conditions for Davies-ENDOR: frequency, 34.1 GHz; temperature, 15 K; RF pulse, 50 μs; inversion pulse, 80 ns; **π**/2,12 ns; **τ** = 300 ns. Condition for Q-band HYSCORE: frequency, 34.1 GHz; temperature, 15 K; **π**/2, 12 ns; **τ** = 368, 392, 388, 368 ns at g = 2.103, 2.075, 2.042, 1.998, respectively; time increment along both dimensions was 24 ns with 270 steps.

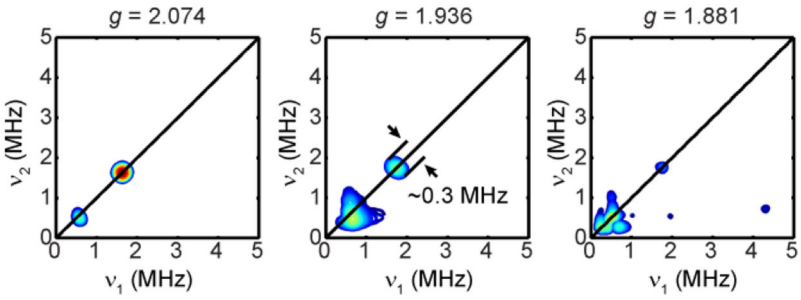

Figure 4.

Q-band HYSCORE spectra of [2^{57}Fe]-*Cr*HydA1 H_{hyd} recorded at three principal *g* values. Conditions: temperature, 10 K; τ = 300 ns; and other settings as indicated in Figure 3.

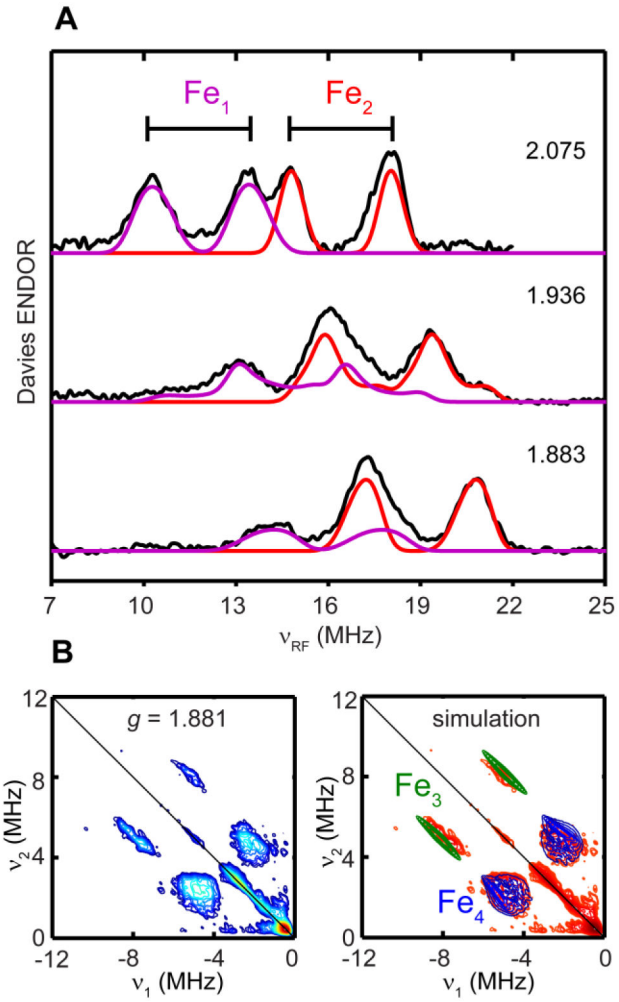

Figure 5.

(**A**) Q-band field-dependent Davies ENDOR spectra of uniformly ^{57}Fe-labeled *Ci*HydA1 (black traces) simulated using two ^{57}Fe *A*-tensors: g = [2.076, 1.936, 1.881]; A $^{57}Fe_1$ = [20.0, 29.5, 35.0] MHz, Euler angle = [140, 35, 40]° (purple traces); A $^{57}Fe_2$ = [35.0, 31.5, 39.5] MHz, Euler angle = [120, 35, 0]° (red traces). (**B**) Q-band HYSCORE spectrum of uniformly ^{57}Fe-labeled *Ci*HydA1 recorded at g_3 = 1.881 (left) and simulation with two ^{57}Fe *A*-tensors (right): g = [2.076, 1.936, 1.881]; A $^{57}Fe_3$ = [20.2, 21.0, 8.5] MHz, Euler angle =[120, 35, 0]° (green contours); A $^{57}Fe_4$ = [16.5, −0.5, 5.5] MHz, Euler angle = [130, 35, 50]° (blue contours). See Figure S8 for HYSCORE spectra and simulations recorded at other g values. Conditions for Davies-ENDOR: frequency, 34.0 GHz; temperature, 10 K; RF pulse, 50 μs; inversion pulse, 80 ns; π/2, 12 ns; τ = 300 ns. Condition for Q-band HYSCORE: frequency, 34.0 GHz; temperature, 10 K; π/2, 12 ns; τ = 300 ns; time increment along both dimensions was 24 ns with 270 steps.

Table 1.

Summary of ^{13}C HFI of the diatomic ligands in different states of the H-cluster

H-cluster state	*A* ^{13}C (MHz)	[α, β, γ] (°)[e]	assignment	reference
H_{ox}[a]	[5.3, 4.0, 4.3]	[25, 25, 0]	CO_p	this work
	[20.5, 29.9, 26.0]	[37, 26, 0]	CO_d	this work
	[9.0, 3.8, 4.5]	[0, 20, 0]	CO_{bridge}	this work
	[5.22, 5.24, 4.16]	[30, 90, 0][f]	CN_p	25
	[30.9, 23.3, 30.2]	[60, 120, 170][f]	CN_d	25
H_{ox}-CO[b]	7.3		CO_p	this work
	[3.2, 3.7, 4.4] 4.8		CO_d	24 this work
	[8.5, 9.8, 3.9] 10.9		CO_{bridge}	24 this work
	[15.6, 16.6, 19.2]; 21[d], 21.1;		$CO_{external}$	24, 26 this work
	[7.2, 7.0, 7.0]	[0, 0, 0]	CN_p	25
	[3.90, 3.75, 3.75]	[0, 0, 0]	CN_d	25
H_{hyd}[c]	[0.30, −0.18, −0.59]	[25, 0, 0]	COp	this work
	[−0.51, 0.16, 0.10]	[35, 0, 0]	CO_{bridge}	this work
	[0.07, 0.17, 0.22]	[0, 10, 0]	CN_p	this work

[a] ^{13}CO HFI are from *Cr*HydA1 H_{ox}; ^{13}CN HFI are from CpI H_{ox}.

[b] ^{13}CO HFI are from *Cr*HydA1 and DdH H_{ox}-CO; ^{13}CN HFI are from CpI H_{ox}-CO.

[c] From *Cr*HydA1 H_{hyd}.

[d] From CpI H_{ox}-CO.

[e] Euler angle are relative to *g*-frame as $g1>g2>g3$.

[f] Euler angles are relative to *g*-frame as $g1<g2<g3$.

Table 2.

Summary of ^{57}Fe HFI of *Cr*HydA1 H-cluster at different states

H-cluster state	*A* ^{57}Fe (MHz)	a_{iso} (MHz)	[α, β, γ] (°)	assignment	reference
H_{ox}	Fe_A: 16–18	~17		Fe_d	[29]
	Fe_B: [10.4, 9.1, 10.2]	9.9	[0, 0, 0]	$[4Fe\text{-}4S]_H$	[29], this work
	Fe_c: [6.5, −1.5, 12.0]	5.7	[17, 50, 25]	Fe_p	this work
	[2.2, 5.5, 5.5]	4.4	[0, 0, 0]	Fe_p	[53]
H_{ox}-CO	[−1.7, 2.8, 2.81	1.3	[0, 15, 0]	Fe_d	[53]
	see ref 51	27.6; 28.0; 30.0; 33.2		$[4Fe\text{-}4S]_H$	[53]
H_{hyd}	<0.3			Fe_p and Fe_d	this work
	Fe_1: [20.0, 29.5, 35.0]	28.2	[140, 35, 40]	$[4Fe\text{-}4S]_H$	this work
	Fe_2: [35.0, 31.5, 39.5]	35.3	[120, 35, 0]		
	Fe_3: [20.2, 21.0, 8.5]	16.6	[125, 35, 0]		
	Fe_4: [16.5, −0.5, 5.5]	7.2	[130, 35, 50]		